Differential Proteomic Analysis of Cancer Stem Cell Properties in Hepatocellular Carcinomas by Isobaric Tag Labeling and Mass Spectrometry

ARTICLE *in* JOURNAL OF PROTEOME RESEARCH · JUNE 2013

Impact Factor: 4.25 · DOI: 10.1021/pr4004294 · Source: PubMed

13 AUTHORS, INCLUDING:

Claire Chiu
National Taiwan Normal University
3 PUBLICATIONS **26** CITATIONS
SEE PROFILE

Hsiang-Wen Tseng
Industrial Technology Research Institute
23 PUBLICATIONS **212** CITATIONS
SEE PROFILE

Journal of proteome research

Article

pubs.acs.org/jpr

Differential Proteomic Analysis of Cancer Stem Cell Properties in Hepatocellular Carcinomas by Isobaric Tag Labeling and Mass Spectrometry

Ching-Huai Ko,[†,‡] Chieh-Fang Cheng,[†,‡] Chin-Pen Lai,[†] Te-Hui Tzu,[§] Chih-Wei Chiu,[§] Mei-Wei Lin,[†] Si-Yuan Wu,[†] Chung-Yuan Sun,[†] Hsiang-Wen Tseng,[‡] Chun-Chung Wang,[‡] Zong-Keng Kuo,[‡] Ling-Mei Wang,[†] and Sung-Fang Chen[§,*]

[†]Strategic Business and Innovation Technology Development Division and [‡]Herbal Medicinal Product Technology Division, Biomedical Technology and Device Research Laboratories, Industrial Technology Research Institute, 195, Sec.4, Chung Hsing Road, Chutung, 31040 Hsinchu, Taiwan; and [§]Department of Chemistry, National Taiwan Normal University, No. 88, Sec. 4, Ting-Chow Road, 116 Taipei, Taiwan

Supporting Information

ABSTRACT: Malignant tumors are relatively resistant to treatment due to their heterogeneous nature, drug resistance, and tendency for metastasis. Recent studies suggest that a subpopulation of cancer cells is responsible for the malignant outcomes. These cells are considered as cancer stem cells (CSC). Although a number of molecules have been identified in different cancer cells as markers for cancer stem cells, no promising markers are currently available for hepatocellular carcinoma cells. In this study, two clones of Hep3B cell lines were functionally characterized as control or CSC-like cells, based on properties including spheroid formation, drug resistance, and tumor initiation. Furthermore, their protein expression profiles were investigated by isobaric tags for relative and absolute quantitation (iTRAQ), and a total of 1,127 proteins were identified and quantified from the combined fractions; 50 proteins exhibited at least 2-fold differences between these two clones. These 50 proteins were analyzed by GeneGo and were found to be associated with liver neoplasms, hepatocellular carcinoma (HCC), and liver diseases. They were also components of metabolic pathways, immune responses, and cytoskeleton remodeling. Among these proteins, the expressions of S100P, S100A14, and vimentin were verified in several HCC cell lines, and their expressions were correlated with tumorigenicity in HCC cell lines. The functional significance of vimentin and S100A14 were also investigated and verified.

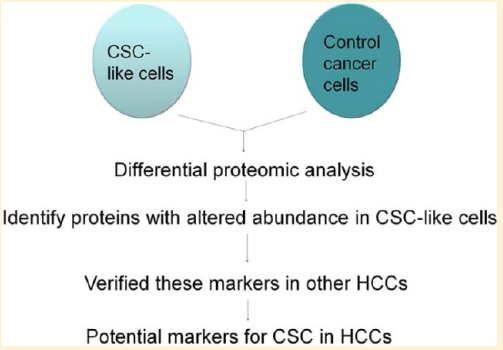

KEYWORDS: *hepatocellular carcinoma, cancer stem cells, proteomic analysis, isobaric tags for relative and absolute quantitation*

INTRODUCTION

Cancer comprises a group of different diseases. In general, cancers result from uncontrolled growth of cells with the formation of malignant tumors. These tumors can invade surrounding tissue and may travel to distant organs or tissues through the circulating system. The development of cancers requires multiple mutations in several cell cycle check points and genes that control cell motility. Therefore, several years to decades may be required before primary tumors can be detected.

Liver cancer is the fifth leading malignancy in men and the ninth in women worldwide.[1] The incidence of liver cancer is highly correlated to chronic local inflammation and cirrhosis. Therefore, chronic hepatitis B and C infections and alcohol overconsumption are considered to be risk factors for liver cancer. Since 80% of the cells in the liver are hepatocytes, hepatocellular carcinoma (HCC) is the most common form of liver cancer.

HCCs are highly aggressive carcinomas, and the majority of patients die within one year after diagnosis without treatment. Conventional treatments include surgery, liver transplantation, and chemotherapy. However, there are restrictions for surgery and liver transplantation, and chemotherapy can be very damaging to a cirrhotic liver. In addition, recurrence is not uncommon after various treatments, and the reasons for this remain unclear.

To explain the high relapse rate of cancers, the heterogenecity of cancer was studied and the theory of tumor initiating cells or cancer stem cells (CSC) was proposed.[2] In brief, spheroid formation *in vitro*, resistance to chemotherapeutic drugs, and the *in vivo* initiation of tumors are included among the criteria for CSC. One of the most extensively studied models for CSC is breast cancer. Breast cancer cells with CD24+/CD44− show high tumor initiating capacities.[3] Although several different cell surface molecules have been reported as CSC markers in different types of cancers, there are no promising CSC markers for hepatocellular carcinoma yet.[4]

Received: May 21, 2012
Published: June 20, 2013

Differential proteomics is an important area of proteomics that involves the comparison and identification of proteins that are expressed by a whole genome or in a complex mixture. The conventional approach is mainly based on 2D-PAGE separation, followed by the identification of differentially expressed proteins by mass spectrometric analysis.

The LC-based approach is becoming increasingly popular since it overcomes the limitations of 2D-PAGE. The sample or the LC-based approach could be based on stable isotope labeling or a label-free approach.[5,6] The label-free LC-MS approach involves measuring and comparing the mass spectrometric ion intensities of a peptide that represents a particular protein. Without isotope tags as internal standards, the results are difficult to interpret and the procedures usually involve additional experimental procedures.

The approach of sobaric tags for relative and absolute quantitation (iTRAQ, Applied Biosystems, Foster City, CA) has attracted considerable attention recently and has been applied in various studies.[7−10] It is a 4-plex (or 8-plex) protein quantitation strategy that utilizes different isotopically tagged reagents attached to primary amine groups at the N-terminus and the side chain of lysine residues. Peptides labeled with these isobaric tags are indistinguishable in the MS survey scan, but fragmentation under MS/MS enables quantitative information to be obtained from low-mass signature ions (m/z from 114 to 117) and regularly fragmented ions (-b, -y types) for protein identification. The advantage of this technology is that it provides the opportunity to study changes in the global proteome and the expression of molecular-level indicators at any time point or treatment.

The theory of CSC was established during the past decade. A large body of evidence now exists to support the existence of CSC-like cells in breast cancer, lung cancer, prostate cancer, colon cancer cells, and liver cancer.[3,11−14] Only a few proteomics studies have been conducted on cancer stem cells to date.[15−18] Although several molecules have been reported to be markers for CSC-like cells in certain HCC cell lines, there are no universal markers reported for HCC, to the best of our knowledge. In the current study, we report on the identification of key indicators for CSC-like cells in HCC by comparing the proteomics of two clones from an identical cell line which showed differential CSC properties. The results were subsequently verified in several other HCC cell lines.

MATERIAL AND METHODS

Cell Cultures

HCC cell lines were purchased from different organizations. Hep3B and HepG2 were purchased from BCRC (Bioresource Collection and Research Center, Taiwan). Huh7 was purchased from JCRB (Japanese Collection of Research Bioresources, Japan). PLC/PRF/5 was purchased from ATCC (American Type Culture Collection, USA). Hep3B and PLC/PRF/5 were cultured in MEMα (Gibco, Carlsbad, CA) with 10% FBS (Gibco), and HepG2 and Huh7 were cultured in DMEM (Gibco) with 10% FBS and Nonessential Amino Acids (Gibco).

Sample Pretreatment and iTRAQ Reagent Labeling

Cells were lysed by using RIPA buffer and PMSF (1 mM), Na-Vanadate (SOV) (1 mM), and proteinase inhibitor cocktail (EMD Millipore, Merck KGaA, Germany). Proteins were enriched using a 3-kDa centrifugal filter as described in the manufacturer's manual (Millipore, Merck KGaA, Germany). Briefly, 100 μL samples were centrifuged at 14,000g for 20 min at 4 °C in the filter tube. The filter device was placed upside down in a clean centrifuge tube and spun for 2 min at 1000g. This process was repeated twice using ddH2O for desalting and protease inhibitor cocktail removal purposes. The amount of protein in each concentrated/desalted sample was determined by the Bradford protein assay (Bio-Rad, Hercules, CA) and stored at −20 °C for subsequent processing.

Protein samples were then reduced, alkylated, digested, and labeled with iTRAQ reagents according to the manufacturer's recommended protocol. The protein pellets were resuspended in 0.5 M triethylammonium bicarbonate (TEAB), pH 8.5, and 0.1% sodium dodecyl sulfate (SDS), reduced with 5 mM Tris (2-carboxyethyl)phosphine (TCEP) for 1 h at 60 °C, and alkylated with 10 mM s-methylmethanethiosulfonate (MMTS) at room temperature for 10 min.

Protein samples (100 μg) from each clone were digested overnight in a tryptic solution (30/1, w/w) at 37 °C. The digested samples were labeled with iTRAQ reagents. Ethanol (70 μL) and the corresponding iTRAQ reagent were added to each sample vial. The samples were labeled as follows: 114 and 116, clone 1; 115 and 117, clone 2 (these two clones are described in the Results and Discussion section). The duplicate sets of iTRAQ samples were performed to verify the consistency of the results. After 1 h of iTRAQ labeling, the samples were then mixed and dried by centrifugal evaporation.

Strong Cation Exchange Chromatography (SCX)

All LC fractionation experiments were performed using an Agilent 1100 Series instrument. The HPLC system consisted of a binary pump, a vacuum degasser, a UV/vis detector set as 214 nm, and a manual injector with a home-calibrated loop (200 μL). All experiments were conducted at 30 °C with a column oven to stabilize the column temperature to ensure reproducibility.

The dried labeled peptide mixtures were reconstituted with buffer A (10 mM KH_2PO_4 in 25% ACN, pH 3). The separation was performed using a PolySULFOETHYL A Column (2.1 mm i.d. × 200 mm L, 5 μm, 300 Å; PolyLC, Columbia, MD) on Agilent 1100 binary HPLC (Agilent Technologies, Wilmington, DE) using a 90 min gradient. iTRAQ labeled peptides (120 g) were eluted at a flow rate of 200 μL/min with a gradient of 2% buffer B (10 mM KH_2PO_4 in 25% ACN/350 mM KCl, pH 3) for 15 min, 2−40% buffer B for 38 min, and 40−98% buffer B for 7 min and then maintained in 98% buffer B for 5 min before equilibrating with 2% buffer B for 20 min. A total of 24 fractions were collected, pooled, and cleaned-up using C-18 Spin columns (Thermo Fisher, San Jose, CA) for further nanoLC-MS/MS analysis.

Basic Reverse-Phase Chromatography

Approximately 120 μg of reconstituted labeled peptides were injected into a BioBasic C18 column (2.1 mm i.d. × 150 mm L, 5 μm, 300 Å; Thermo Scientific). All runs were operated at a flow rate of 200 μL/min, and temperature was held at 37 °C. The basic RP-HPLC buffers consisted of buffer A (50 mM NH_4OH in H_2O, pH 8.44) and buffer B (50 mM NH_4OH in 80% ACN, pH 8.45). The gradient was 2% buffer B for 20 min, 3−60% buffer B in 50 min, and then maintained in 98% buffer B for 10 min before equilibrating with 2% buffer B for 15 min. A total of 24 fractions were collected and pooled for further nanoLC-MS/MS analysis.

Solution IEF

iTRAQ dried labeled peptide (120 g) was dissolved in 0.72 mL of ddH_2O and 2.88 mL of IPG stock buffer (pH 3−10). The IPG strips (pH 3−10, 24 cm) were assembled on the OGE trays and rehydrated for 30 min with a solution of 240 μL of H_2O and

dx.doi.org/10.1021/pr4004294 | J. Proteome Res. 2013, 12, 3573−3585

0.96 mL of IPD stock buffer. The samples were loaded on 24 off-gel wells. The separation was carried out over a 48 h period using a 3100 OFFGEL fractionator (Agilent Technologies) with a limiting current of 50 μA and a limit of 50 kV·h before holding the voltage at 500 V. The samples from the collected fractions were cleaned-up using C-18 Spin columns for further nanoLC-MS/MS analysis.

LC-ESI-MS/MS Analysis

All iTRAQ samples from the fractions were dried by speed vacuuming and stored at −20 °C. Prior to reverse-phased nanoLC/MS/MS analysis, these fractions were redissolved in 20 μL buffer that contained 5% acetonitrile and 0.1% formic acid. A total of 1.4 μL of each sample was injected onto a 300 μm i.d. × 1 mm L nanoprecolumn at a flow rate of 20 μL/min with a loading time of 10 min for preconcentration and cleanup. Reverse phase separation of the labeled peptide mixture was performed in a nanoHPLC system (Agilent Technologies) using a C-18 column (75 μm i.d., 150 mm L, 3 μm particles) at a flow rate of 200 nL/min. The solvent system was as follows: solvent A was 0.1% (w/v) formic acid/H_2O/2% (v/v) acetonitrile, and solvent B was 0.1% (w/v) formic acid/H_2O/80% (v/v) acetonitrile. The gradient was isocratic with 2% solvent B, eluted with a linear gradient from 2% solvent B to 60% solvent B over 90 min; the column was then washed using 80% solvent B for 10 min and rebalanced with buffer A for 15 min. The nanoHPLC system was connected online to a hybrid LC-MS/MS system (Applied Biosystems API QSTAR XL, MA). Online MS and tandem MS spectra were obtained using the TOF analyzer with m/z scanning ranges of 400−1200 Da for MS and 75−1500 Da for MS/MS analyses. The information-dependent acquisition (IDA) automatically determined the three most intense ions with multiple charges (+2 ∼ +3) in a TOF/MS survey scan. The optimized MS/MS experiments were performed on the selected ions.

Database Search and iTRAQ Quantification

The MS/MS data were analyzed for identification and quantitation using Mascot Daemon (Matrix Science, London, U.K.; version 2.2.1) and ProteinPilot (Applied Biosystems, USA; version 2.0.1). The false discovery rate was calculated by Mascot after searching against a decoy database. Search parameters included trypsin as the enzyme with one missed cleavage allowed; methyl methanethiosulfonate at cystenine and iTRAQ 4-plex at lysine and the N-terminal residue were set as fixed modifications while oxidation at methionine and iTRAQ 4-plex at tyrosine were set as variable modifications. Fragment ion mass tolerance and precursor ion tolerance were set to 0.20 Da. All tandem mass spectra were searched for species of *Homo sapiens* against the Swiss-Prot (release-2011_04) containing 526969 sequences using ProteinPilot 2.0.1 Software (Applied Biosystems) for quantification. The accuracy tolerance for both peptides and peptide fragments was set to 0.2 Da with a 95% confidence threshold. To designate significant changes in protein expression, fold changes >2.0 or <0.5 were set as cutoff values. In order to decrease the artificial error, the bias correction option was executed.

Western Blot

Total cellular lysates were prepared using RIPA lysis buffer. Proteins in cell lysates (40 μg) were separated on 10% SDS-polyacrylamide minigels and electrotransferred to a PVDF membrane by an iBlot Dry Blotting System (Invitrogen, Carlsbad, CA). The antibodies used were as follows: S100A11 (Abcam, ab82850), S100A14 (Proteintech, 10489-1-AP), S100P (Cell signaling, 7677S), Vimentin (BD, 550513), Beta-actin (Novus, NB600-501).

FACS Analysis

Cells were incubated with dye-labeled monoclonal antibodies CD13 (BD), CD24 (BD), CD44 (MACS), CD90 (BD), CD133 (MACS), c-KIT (MACS), EpCAM (MACS), Vimentin (EXBIO), and KRT19 (Abcam) for 30 min on ice. The stained cells were then washed twice and resuspended in cold buffer and analyzed by FACScan flow cytometry (Becton Dickinson, San Jose, CA). More than 1×10^5 cells were analyzed for each sample, and the results were processed by means of the WinMDI 2.8 software (Scripps Research Institute, La Jolla, CA).

Real-Time Reverse Transcription−Polymerase Chain Reaction (RT-PCR)

For real-time RT-PCR analysis, the total RNA was extracted from the cells using an RNeasy Mini Kit (Qiagen). DNA was eliminated by treatment with Deoxyribonuclease I (Invitrogen). Briefly, the total RNA (2 μg) of each sample was reverse transcribed with 0.5 μg of oligo dT and 200 U SuperScript III RT (Invitrogen) in a 20 μL reaction. PCR was carried out with a StepOnePlus Real-Time PCR System (ABI) in a total volume of 25 μL containing 0.5 mM of each primer, 1× Power SYBR Green PCR Master Mix (Life Technologies), and 50 ng of cDNA. The quantification of the unknown samples was performed by StepOne Software, version 2.0 (ABI). GAPDH was amplified as a reference standard in each experiment. The primers used are as follows: S100A4 (F), TCTCTCCTCAGCTTCTTC; S100A4 (R), GCTGTCCAAGTTGCTCATCA; S100A10 (F), AAATTCGCTGGGGATAAAGG; S100A10 (R), AGCCCACTTTGCCATCTCTA; S100A11(F), CCAACATGGCAAAAATCTCC; S100A11 (R), CCATCACTGTTGGTGTCCAG; S100A14 (F), CTGACCCCTTCTGAGCTACG; S100A14 (R), CCAGAGGGAGTTCTCAGTGC; S100P (F), TACCAGGCTTCCTGCAGAGT; S100P (R), CTCCAGGGCATCATTTGAGT; Vimentin (F), GAGAACTTTGCCGTTGAAGC; Vimentin (R), TCCAGCAGCTTCCTGTAGGT; GAPDH (F), GAAGGTGAAGGTCGGAGT; GAPDH (R), GAAGATGGTGATGGGATTTC.

Spheroid Formation Assay

The HCC cells were cultured in serum-free DMEM/F12 (Gibco) with N2 supplement (Gibco), 10 ng/mL human recombinant bFGF (R&D Systems), and 10 ng/mL EGF (R&D Systems) at 1×10^5/mL in low-attachment 96-well plates (Corning). Images were obtained every other day to observe the formation of spheroids. The numbers of spheroids formed were counted to quantify spheroid formation in each cell line.

Wound Healing Assay (*in Vitro*)

Migration was tested by *in vitro* wound healing assays with Culture inserts (ibidi). Cells were seeded in 6-well plates with Culture inserts ($(1-2) \times 10^5$ cells/mL). After cells attached, cells were starved in serum-free medium overnight and then treated with 25 μg/mL of Mitomycin-C (Kyowa Kirin) at 37 °C for 20 min. Culture inserts were removed, and cells were incubated at 37 °C and 5% CO_2. Images of the cell-free area were obtained at 0, 24, and 48 h after the removal of culture inserts. Cell motility was quantified by measuring the reduced cell-free area based on the obtained images.

Viability Assay (MTT)

Cells were seeded at 10^4 cells in 100 μL of medium per well in a 96 well plate and incubated (37 °C, 5% CO_2) overnight. Drugs of interest were added to each well and incubated (37 °C, 5% CO_2) for 2 days. MTT solution (5 mg/mL, Sigma) was added to each well at a final concentration of 0.5 mg/mL, followed by

dx.doi.org/10.1021/pr4004294 | J. Proteome Res. 2013, 12, 3573−3585

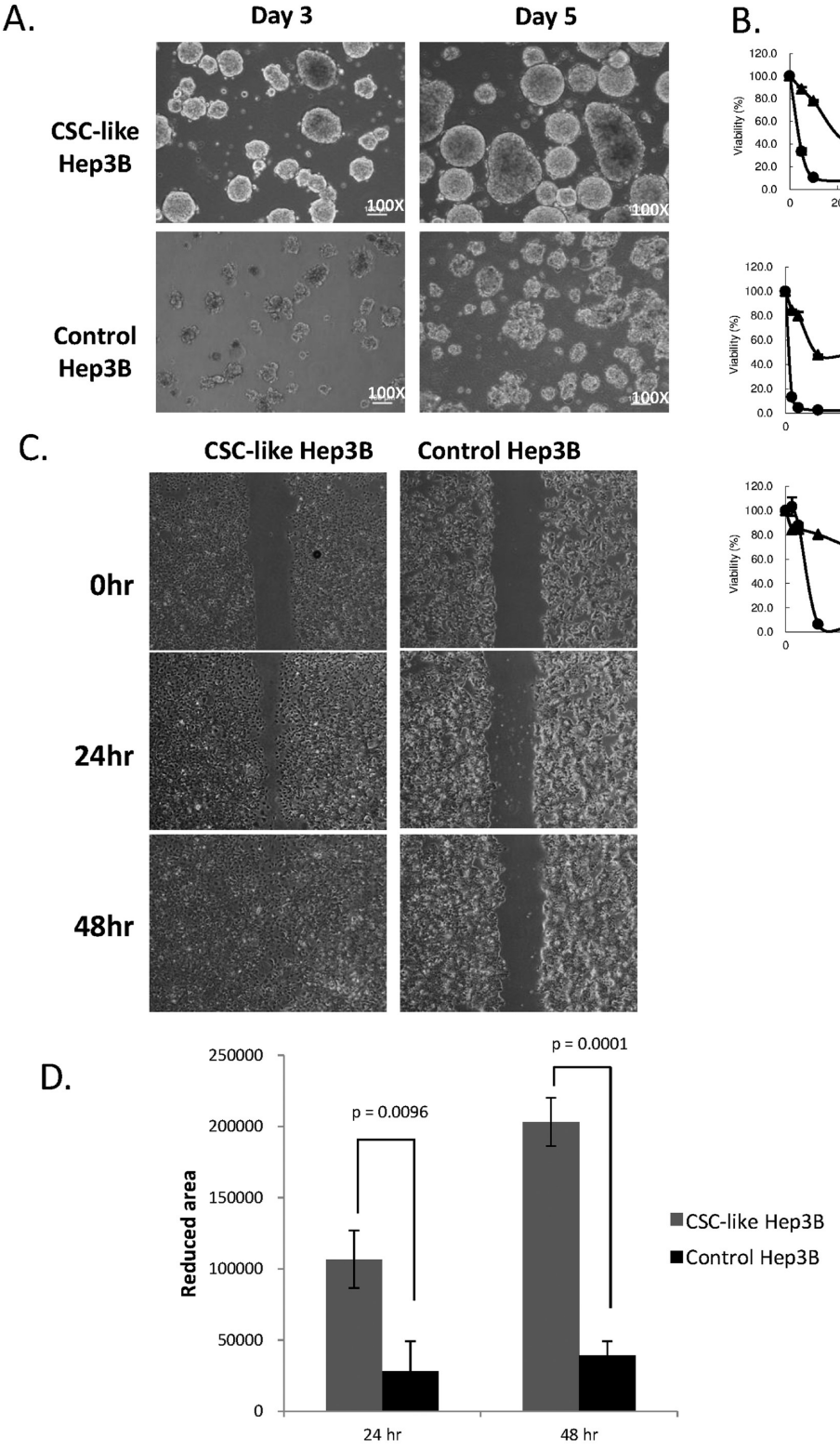

Figure 1. Analysis of CSC properties in Hep3B clone 1 and clone 2. (A) Images of spheroids formed by Hep3B clone 1 and 2 were observed 3 and 5 days after the cells were plated. Spheroids were broken up on day 5 and were used to analyze cell viability with an Adam Automatic Cell Counter. (B) Three chemotherapeutic reagents were used to treat the two clones of Hep3B for 2 days. Cell viability was tested by using an MTT assay. (C) Cell motility of the two clones of Hep3B was evaluated with a scratch assay. Images of scratch assays were taken at 0 h, 24 h, and 48 h post-scratch. (D) Scratched area was quantified with a computer-based analysis system ($N = 3$, $^*p < 0.05$).

incubation (37 °C, 5% CO_2) for 1−2 h. Afterward, 100 μL of 10% SDS (Fluka) was added to each well and incubated at room temperature overnight. The optical density at 570 nm was detected with a SpectraMax M5 (Molecular Devices) to quantify the results.

RNA Interference

S100A14 siRNAs were purchased from GeneDireX. The antisense sequences of these siRNAs were as follows: S100A14-1, CCCUC-AUCA AGA ACUUUCACCAGUA; S100A14-2, GACUCUAA-

dx.doi.org/10.1021/pr4004294 | J. Proteome Res. 2013, 12, 3573−3585

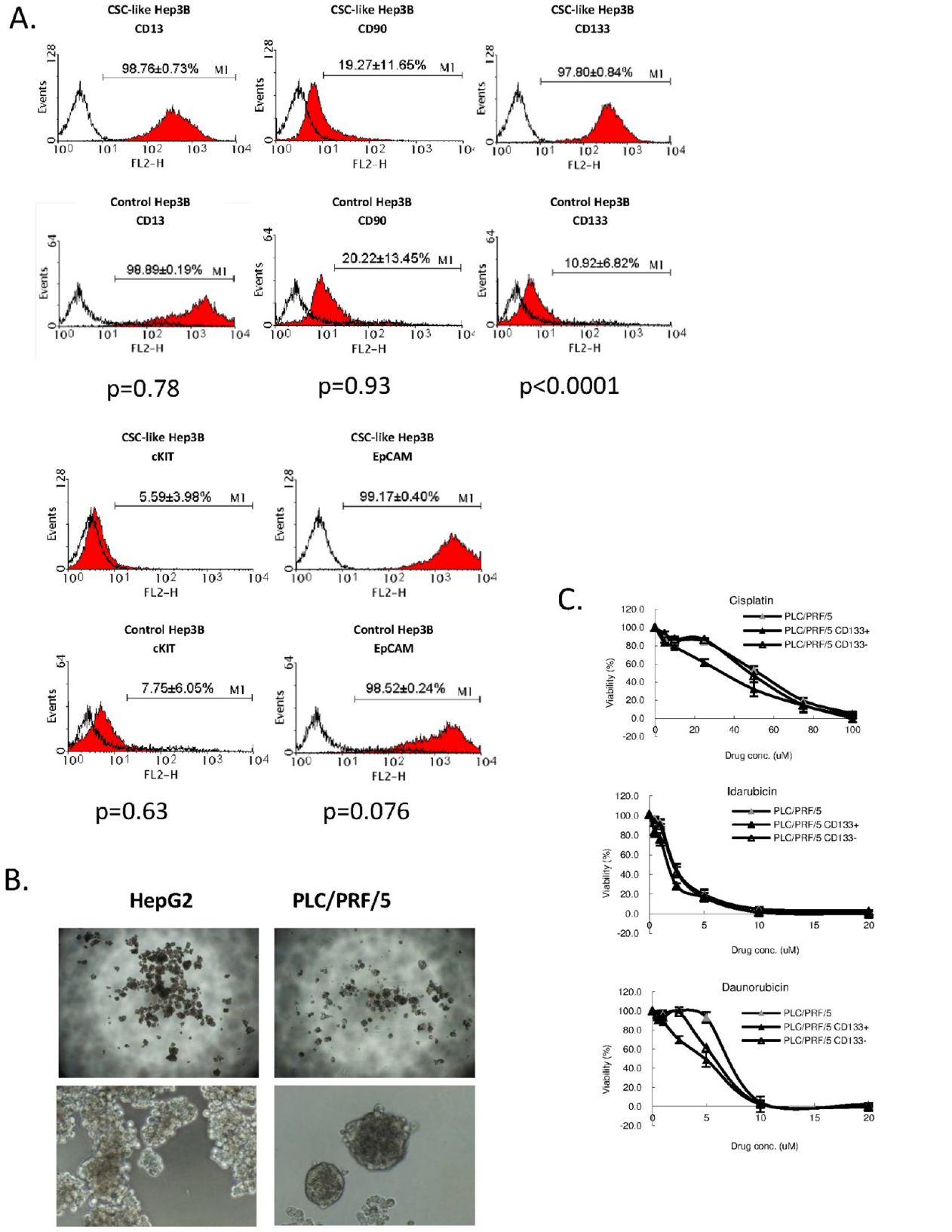

Figure 2. CD133 is not a universal CSC marker in HCC. (A) The expressions of reported CSC markers on the two clones of Hep3B were analyzed by FACS ($N = 3$). (B) PLC/PRF/5 and HepG2 cells were incubated in a low-attachment cultural environment for 5 days. Images of speroids formed by these cells were taken to compare the speroid forming ability of these cell lines. (C) Three chemotherapeutic reagents were used to treat parental or sorted (CD133+ or CD133−) PLC/PRF/5 cells for 2 days. Cell viability was tested by using the MTT assay.

ACUGGAGUUCAGGAGUU; and S100A14-3, GGGUCUUU-AAGAACCUACUUCCUAA. The siRNA duplexes were transiently transfected to HCC cells with lipofectamine 2000 (Cat. No. 11668-019, Invitrogen) according to the manufacturer's protocol.

dx.doi.org/10.1021/pr4004294 | J. Proteome Res. 2013, 12, 3573−3585

Table 1. Summary for the Expression of CSC Markers in HCC Cell Lines[a]

	CSC-like Hep3B (%)	control Hep3B (%)	PLC/PRF/5(%)	HepG2 (%)
CD13	>90	>90	50−90	>90
CD90	10−50	10−50	10−50	10−50
CD133	>90	10−50	10−50	10−50
cKit	<10	<10	<10	<10
EpCAM	>90	>90	<10	>90

[a]Expression of CSC markers in CSC-like Hep3B, control Hep3B, PLC/PRF/5, and HepG2 cells was detected with a flow cytometer. Numbers in the table represent the percentage of cells that express the corresponding markers (N = 3).

Table 2. Tumor Initiating Activities of Parental and Sorted (CD133+ and CD133-) PLC/PRF/5 and Huh-7 Cells in SCID Mice[a]

	marker	cell no.	no. of mice w/tumor on day 60
Huh-7	parental	1×10^5	3/3
	CD133+	1×10^5	2/3
	CD133-	1×10^5	3/3
PLC/PRF/5	parental	3×10^3; 1×10^4	5/5; 5/5
	CD133+	3×10^3 ; 1×10^4	5/6; 5/5
	CD133-	3×10^3 ; 1×10^4	5/6; 5/5

[a]Equal numbers of parental, CD133+, and CD133- HCC cells (PLC/PRF/5 or Huh-7) were injected in SCID mice for tumorigenicity analysis. Tumor sizes were measured weekly, and numbers of mice bearing tumors on day 60 after tumor injection were shown here.

In Vivo Tumorigenicity Assay of Xenograft Tumor Model

All experimental protocols were approved by the Institutional Animal Care and Use Committee (IACUC No. ITRI-IACUC-2010-026R, Industrial Technology Research Institute of Taiwan, HsinChu, Taiwan). SCID (CB17/Icr-Prkdcscid/CrlBltw) mice were purchased from LASCO Ltd. (Ilan, Taiwan). Different amounts of PLC/PRF/5 cells in 100 μL of mix (equal volumes of PBS and Matrigel) were implanted subcutaneously (sc.) into the right flank of female SCID mice. Tumor sizes were measured with calipers and tumor volumes (V) calculated by the following formula: $V = LS2/2$ (where L is the longest diameter and S is the shortest diameter).

Pathway and Disease Biomarker Enrichment Analysis

The selected targets were matched to the Go database (MetaCore TM) for analysis. According to the instruction of MetaCore TM, the probability of a random intersection between a set of IDs and a targets list with ontology entities is estimated by the p value of the hypergeometric intersection. The lower p value means higher relevance of the entity to the data set, which shows in a higher rating for the entity. The pathway map database contains a set of roughly 650 signaling and metabolic maps covering human biology. The disease biomarker analysis database contains data in over 500 human diseases with gene content annotated by GeneGo. After uploading the gene symbols of differentially expressed proteins into MetaCore TM, the "Statistically significant Map" and "Statistically significant Diseases" were estimated and sorted by p value.

Statistical Analysis

Data were analyzed by Student's t-test and considered statistically significant if $P < 0.05$. All data were mean ± SEM of three independent experiments unless indicated otherwise.

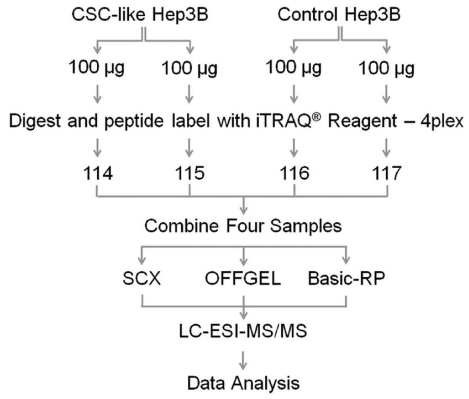

Figure 3. The work pipeline for the Hep3B cancer stem cells study. Hep3B samples were subjected to tryptic digestion, labeled with iTRAQ reagents, and combined for fractionation, followed by LC-MS/MS and data analysis.

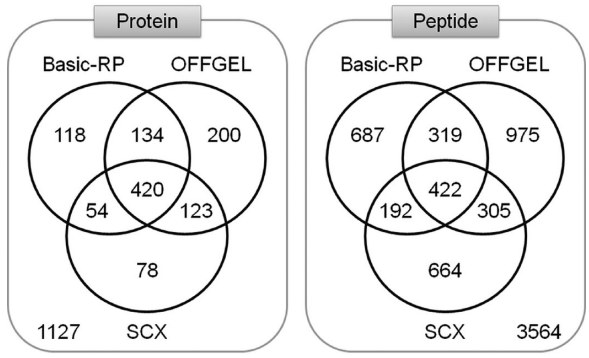

Figure 4. Venn diagrams of (A) identified proteins and (B) unique peptides overlapping between fractionation strategies. Three fractionation strategies were compared, including SCX, basic RP, and solution IEF (OFFGEL). There were 3564 peptides that were associated with the 1127 proteins identified in this study.

RESULTS AND DISCUSSION

Select Hep3B Cells with High or Low Spheroid Formation Properties

When culturing Hep3B cells, we observed that a certain portion of Hep3B cells formed spheroids spontaneously. To study the difference between spheroid-forming and adhesive Hep3B cells, we separated these two types of cells and replated them into tissue culture dishes. After several rounds of enrichment, we collected spheroid-forming Hep3B cells as clone 1 and adhesive Hep3B cells as clone 2. The growth rates of these two clones were different. Hep3B clone 2 cells grew faster compared to clone 1 cells. The doubling time of Hep3B clone 1 cells was 46.97 h, while the doubling time of Hep3B clone 2 cells was 37.72 h. The spheroid-forming properties of these two clones were verified in a low-attachment cultural environment. The Hep3B clone 1 formed spheroids within 3 days after being plated, while the Hep3B clone 2 did not survive well in the low attachment cultural environment (Figure 1A). The viabilities of Hep3B clone 1 and clone 2 in low attachment dishes for 5 days were 91% and 33%, respectively.

To further determine the tumor initiating properties of these two clones, the drug resistance of these two clones against several chemotherapeutic agents, including cisplatin, daunorubicin, and idarubicin was examined. While the cell viability of the Hep3B clone 2 was suppressed at low concentrations of chemotherapeutic agents, the Hep3B clone 1 was more resistant to

dx.doi.org/10.1021/pr4004294 | J. Proteome Res. 2013, 12, 3573−3585

Table 3. Summary of Proteins with Differential Protein Expression Ratio between Different Hep3B Clones

N	accession no.	gene symb	ProtScore	seq cov (%)	no. unique pept	115:114	*p* value 115:114	117:116	*p* value 117:116	full name
(A) The 20 Up-Regulated Genes Expressed More than Two Fold in CSC-like Hep3B Cells When Compared to Control Hep3B Cells										
27	P00352	AL1A1	44.14	55.09	37	2.426459789	0	2.492429495	1.60×10^{-41}	retinal dehydrogenase 1
49	Q00610	CLH1	34.01	12.36	72	2.008279085	3.55×10^{-25}	2.26295495	1.13×10^{-15}	clathrin heavy chain 1
62	P15311	EZRI	30.68	22.87	32	3.111442327	1.07×10^{-14}	3.009198904	2.58×10^{-12}	ezrin
89	P67936	TPM4	25.46	34.27	30	2.441954374	1.01×10^{-8}	2.513000965	2.09×10^{-9}	tropomyosin α-4 chain
107	P21333	FLNA	21.39	3.93	68	3.212021351	1.17×10^{-5}	2.803719997	0.000980878	filamin-A
163	O43175	SERA	16.70	20.64	25	2.737963438	3.79×10^{-9}	2.726233959	4.67×10^{-9}	D-3-phosphoglycerate dehydrogenase
176	P09493	TPM1	22.74	34.51	28	3.273453474	1.24×10^{-6}	3.015184879	6.02×10^{-5}	tropomyosin α-1 chain
240	O60664	PLIN3	12.07	23.27	16	2.872314692	9.53×10^{-6}	3.018698931	1.84×10^{-5}	perilipin-3
322	P37802	TAGL2	9.65	30.15	17	2.838307142	5.20×10^{-11}	3.127317905	6.27×10^{-8}	transgelin-2
333	Q16658	FSCN1	9.22	13.39	21	3.607423067	9.41×10^{-5}	3.164020777	9.80×10^{-5}	fascin
406	P78417	GSTO1	7.72	14.52	13	2.091352463	1.90×10^{-11}	2.909086227	0.000410282	glutathione s-transferase omega-1
428	P09936	UCHL1	7.40	18.83	12	5.621177197	8.75×10^{-9}	4.873823643	2.26×10^{-5}	ubiquitin carboxyl-terminal hydrolase isozyme L1
569	Q53GQ0	DHB12	5.20	9.29	11	3.648901224	7.15×10^{-5}	3.751333952	7.09×10^{-5}	estradiol 17-β-dehydrogenase 12
671	P48147	PPCE	4.04	2.96	13	3.174550533	0.000393092	3.652472019	0.006318464	prolyl endopeptidase
707	P57088	TMM33	4.00	8.50	4	2.065327168	1.05×10^{-5}	2.109095097	0.000129558	transmembrane protein 33
813	P21964	COMT	3.00	5.53	8	3.134186029	0.002337544	2.87791276	0.007599287	catechol *O*-methyltransferase
966	Q99856	ARI3A	2.08	3.04	15	2.433027983	4.92×10^{-5}	2.31163764	0.011393955	AT-rich interactive domain-containing protein 3A
1040	P63313	TYB10	3.01	31.82	4	3.341143608	0.013491944	3.892924786	0.004147051	thymosin β-10
1182	P22061	PIMT	2.00	7.49	4	2.810184956	0.008276392	2.578795433	0.015831169	protein-L-isoaspartate(D-aspartate) *O*-methyltransferase
1230	P11717	MPRI	1.71	0.40	30	2.151643276	0.005016737	2.113700628	0.021969413	cation-independent mannose-6-phosphate receptor
B. The 30 Down-Regulated Genes Expressed Less than 0.5 Fold in CSC-like Hep3B Cells When Compared to Control Hep3B Cells										
48	Q04828	AK1C1	34.54	57.59	34	0.198670313	3.54×10^{-7}	0.176297948	5.64×10^{-8}	aldo-keto reductase family 1 member C1
152	P22309	UD11	17.53	25.70	18	0.220497265	1.60×10^{-8}	0.204589382	9.60×10^{-11}	UDP-glucuronosyltransferase 1−1
168	P24752	THIL	16.61	22.95	25	0.422809511	8.78×10^{-7}	0.428195357	3.42×10^{-6}	acetyl-CoA acetyltransferase, mitochondrial
175	P31327	CPSM	16.33	6.93	33	0.214429408	3.21×10^{-6}	0.218514889	2.22×10^{-6}	carbamoyl-phosphate synthase [ammonia], mitochondrial
177	P16435	NCPR	16.26	17.28	24	0.467154711	1.99×10^{-6}	0.458413661	2.38×10^{-6}	NADPH−cytochrome P450 reductase
264	O95994	AGR2	10.94	44.57	8	0.167761639	2.74×10^{-7}	0.158800259	5.88×10^{-10}	anterior gradient protein 2 homologue
286	Q13162	PRDX4	12.59	31.73	15	0.409673125	8.72×10^{-9}	0.395405203	6.74×10^{-10}	peroxiredoxin-4
369	P29401	TKT	8.32	10.27	31	0.465415716	2.00×10^{-7}	0.463372529	4.76×10^{-7}	transketolase
391	P52895	AK1C2	30.53	54.49	26	0.133793667	9.23×10^{-6}	0.112320893	7.76×10^{-6}	aldo-keto reductase family 1 member C2
425	O60488	ACSL4	11.38	9.42	24	0.415440112	1.45×10^{-8}	0.406431347	6.73×10^{-7}	long-chain-fatty-acid–CoA ligase 4
430	Q6PI48	SYDM	7.35	3.10	23	0.461699843	0.011958743	0.411997765	0.000632678	aspartyl-tRNA synthetase, mitochondrial
445	P00480	OTC	6.79	13.84	16	0.220647991	0.016486991	0.206084639	0.007081501	ornithine carbamoyltransferase, mitochondrial
527	P27338	AOFB	5.77	5.38	15	0.363243759	0.003072235	0.350281596	0.004219316	amine oxidase [flavin-containing] B
534	P55157	MTP	5.71	3.36	19	0.279862642	0.001017605	0.408397138	0.001029626	microsomal triglyceride transfer protein large subunit
631	Q04837	SSBP	4.34	20.27	12	0.419117302	0.00603895	0.403810889	0.002449517	single-stranded DNA-binding protein, mitochondrial
641	O75340	PDCD6	4.26	10.99	8	0.37442863	0.004139354	0.43504411	0.002783685	programmed cell death protein 6
682	P60903	S10AA	4.02	35.05	8	0.340846628	0.015430491	0.343516231	0.002910172	protein S100-A10
698	O75131	CPNE3	4.00	3.54	8	0.423647583	0.005385413	0.35024178	0.002369491	copine-3
710	O14880	MGST3	4.00	13.82	3	0.323817343	0.003282824	0.413291097	0.019706478	microsomal glutathione S-transferase 3
716	P31949	S10AB	3.92	15.24	6	0.166034669	1.69×10^{-6}	0.226011038	5.13×10^{-5}	protein S100-A11
733	P05026	AT1B1	3.70	6.60	9	0.46164155	0.00057553	0.48629427	0.00032778	sodium/potassium-transporting ATPase subunit β-1

dx.doi.org/10.1021/pr4004294 | *J. Proteome Res.* 2013, 12, 3573−3585

Table 3. continued

N	accession no.	gene symb	ProtScore	seq cov (%)	no. unique pept	115:114	p value 115:114	117:116	p value 117:116	full name
(A) The 20 Up-Regulated Genes Expressed More than Two Fold in CSC-like Hep3B Cells When Compared to Control Hep3B Cells										
738	P04181	OAT	4.00	2.96	17	0.359712154	0.005504087	0.252803653	0.01277348	ornithine aminotransferase, mitochondrial
779	Q9Y305	ACOT9	3.30	8.20	9	0.296848238	0.019688547	0.304204613	0.005842746	acyl-coenzyme A thioesterase 9, mitochondrial
789	Q9UBM7	DHCR7	3.22	1.68	10	0.383384049	1.22×10^{-6}	0.40489769	3.08×10^{-6}	7-dehydrocholesterol reductase
819	P15144	AMPN	2.97	1.55	17	0.41430518	0.039572533	0.40728265	0.020777512	aminopeptidase N
989	P49821	NDUV1	2.06	2.80	11	0.486151397	0.017705552	0.444910288	0.006485573	NADH dehydrogenase [ubiquinone] flavoprotein 1, mitochondrial
1161	P36551	HEM6	2.00	1.98	6	0.463724911	0.005241694	0.45443213	0.010593591	coproporphyrinogen-III oxidase, mitochondrial
1163	O15427	MOT4	2.00	2.80	6	0.484193295	0.040395319	0.43216756	0.010240561	monocarboxylate transporter 4
1180	Q15125	EBP	2.00	5.22	4	0.203781396	0.032707967	0.276855588	0.024566336	3-β-hydroxysteroid-δ(8),δ(7)-isomerase
1185	O00625	PIR	2.00	4.14	4	0.486160159	0.008155988	0.473436475	0.003807992	Pirin
B. The 30 Down-Regulated Genes Expressed Less than 0.5 Fold in CSC-like Hep3B Cells When Compared to Control Hep3B Cells										

these drugs (Figure 1B). These results suggested that the Hep3B clone 1 cells fulfilled the criteria for CSC, whereas Hep3B clone 2 did not.

Cell Motility of the Two Clones of Hep3B

It was predicted that CSCs are responsible for cancer metastasis in addition to their role in maintaining tumor growth, and the relationship between CSC-like cells and metastasis has been demonstrated in the case of pancreatic cancer.[19,20] Cell migration is an important step for cancer metastasis. To clarify the role of CSC-like cells in cancer metastasis, cell migration was monitored using the CSC-like Hep3B (clone 1) and control Hep3B (clone 2) by *in vitro* wound healing assay. As expected, CSC-like Hep3B migrated in response to serum while control Hep3B did not (Figure 1C and D).

Expression of Stemness Markers in HCCs

Several cell surface markers were reported as markers for cancer stem cells (CSC) in different types of cancers. To study the expression profiles of the markers, we monitored the expression levels of several markers with specific antibodies in the two clones of Hep3B cells by FACS analysis. Among those markers, CD133 was expressed at higher levels in CSC-like Hep3B compared to control Hep3B cells. Other markers were expressed at similar levels in these two clones of Hep3B. Furthermore, the expressions of these CSC markers were also examined in two other HCC cell lines: HepG2 and PLC/PRF/5 (Figure 2A; Table 1; Supporting Information (SI) Table 1). The ability of spheroid formation was tested in both HepG2 and PLC/PRF/5 cells. As shown in Figure 2B, PLC/PRF/5 but not HepG2 cells formed spheroids within 5 days in a low attachment cultural environment.

To verify if CD133 is critical for the CSC property of HCC, we separated CD133+ and CD133− PLC/PRF/5 cells by cell sorting and examined the drug resistance of parental and CD133 sorted PLC/PRF/5 cells. The expression of CD133 did not affect the drug resistance of PLC/PRF/5 cells (Figure 2C).

Additionally, we separated CD133+ and CD133− cells in Huh7 and PLC/PRF/5 cells. Parental and sorted cells were injected into SCID mice subcutaneously to observe tumor growth *in vivo*. However, the expression of CD133 did not affect the *in vivo* tumor growth of Huh7 and PLC/PRF/5 cells (Table 2).

The results above suggested that CD133 is not a universal marker for CSC in HCC. Therefore, we sought to identify novel markers for CSC in HCC by proteomic assays. We performed iTRAQ analysis for proteomic expression profiles to identify novel CSC markers in HCC cells.

Experimental Design and Proteomic Results of These Two Clones of Hep3B

Since the two clones of Hep3B showed different CSC properties, protein expression profiles of these two clones were investigated using the iTRAQ approach. The work pipeline of this study is demonstrated in Figure 3, and an example an MS/MS spectrum of an iTRAQ-labeled peptide is demonstrated in SI Figure 1. Detailed procedures were as described in the Materials and Methods section.

A total of 1127 proteins were identified with 2.13% FDR using the MASCOT search algorithm (Matrix Science, U.K.). There were 1323, 1436, and 1673 peptides identified in the SCX, basic RP, and solution IEF fractions, corresponding to 623, 674, and 813 proteins, respectively. Similar results were obtained when the data were analyzed by ProteinPilot, which was the principle method for quantitative analysis (SI Figure 2). It is noteworthy that solution-IEF did not contain the most spectra identified but

dx.doi.org/10.1021/pr4004294 | J. Proteome Res. 2013, 12, 3573−3585

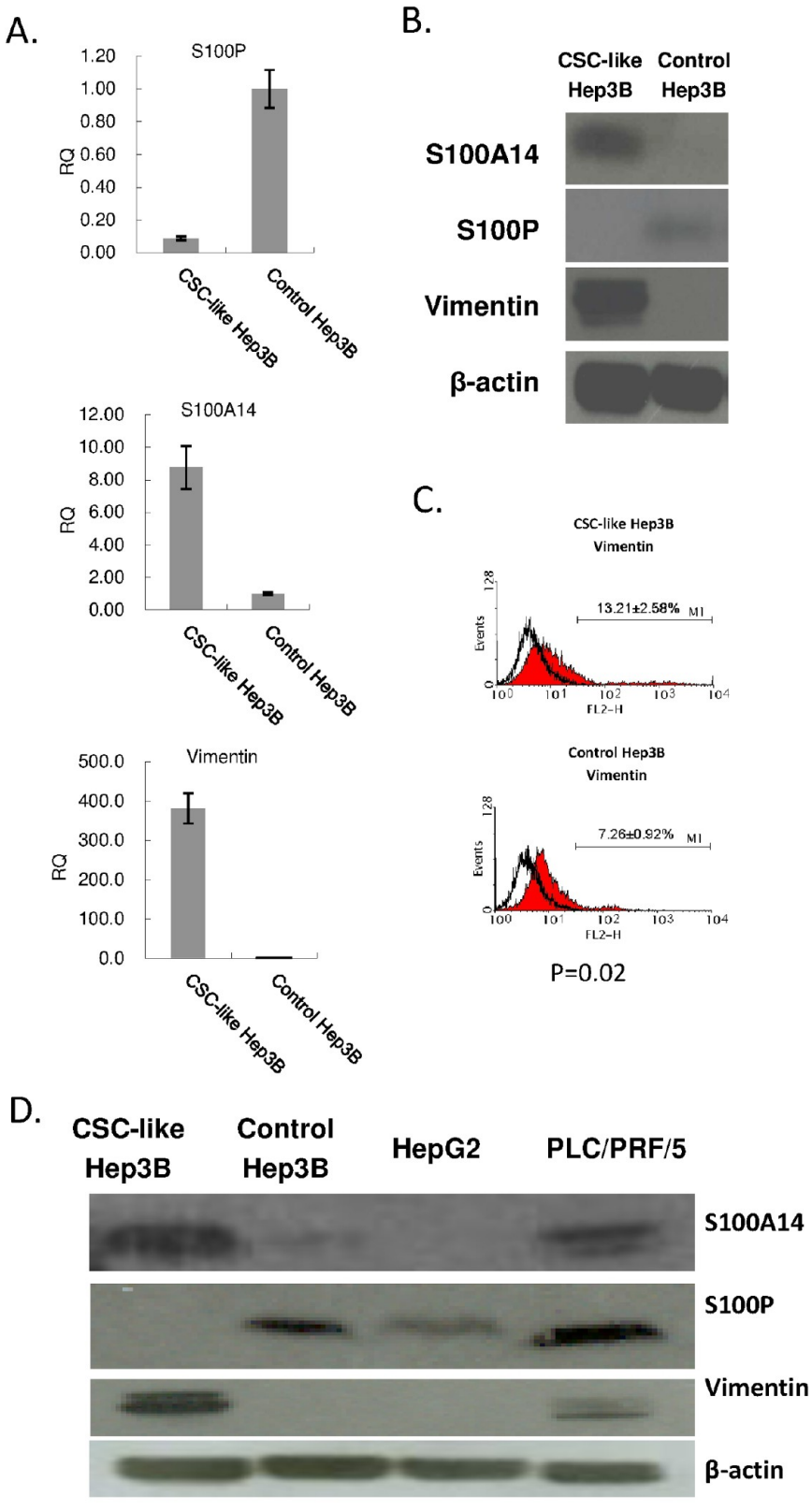

Figure 5. Expression level of CSC-related proteins identified by iTRAQ. (A) The mRNA expression levels of CSC-related proteins in the two clones of Hep3B identified by iTRAQ were verified by QRT-PCR. GAPDH was used as internal control (RQ: Relative Quantitation). (B−C) The protein levels of CSC-related proteins in the two clones of Hep3B identified by iTRAQ were verified by Western blot (B), or FACS analysis (C) ($N = 3$). (D) The expression levels of S100P, S100A14, and Vimentin were tested in HepG2 and PLC/PRF/5 in addition to the two clones of Hep3B. Representative images of three independent experiments are shown.

contained the most proteins identified, although these differences were not significant. Several factors, including fractionation resolution, orthogonality, and peptide recovery after the desalting procedure, may influence the outcome of the analysis.

dx.doi.org/10.1021/pr4004294 | J. Proteome Res. 2013, 12, 3573−3585

Table 4. Summary of HCC Cell Lines Drug Resistance against Chemotherapeutic Agents[a]

	CSC-like Hep3B	control Hep3B	HepG2	PLC/PRF/5
cisplatin	>12.5	2.67 ± 1.58*	12.15 ± 2.22	63.90 ± 7.34
daunorubicin	>20	3.10 ± 0.50*	7.97 ± 5.01*	>20
idarubicin	1.74 ± 0.00	0.19 ± 0.05*	1.45 ± 0.62	2.26 ± 0.56

[a]Numbers represent IC50 (μM) of cisplatin, daunorubicin, and idarubicin on the two clones of Hep3B, HepG2, and PLC/PRF/5 cell line ($N = 3$; *$p < 0.05$ compared to corresponding treatment on Hep3B clone 1 cells).

We examined the number of peptides in 24 collected fractions and their distribution. The results obtained from SCX, basic RP, and solution IEF are summarized in SI Figure 3. All three strategies demonstrated good fractionation capability. The resolution for SCX was the lowest, with 55.4% of the peptides in a single fraction identified. There were 86.7% and 84.5% of the peptides identified from basic RP and solution-IEF located in a single fraction, respectively. When two adjacent fractions combined were considered, 75.6%, 96.4%, and 95.2% of the peptides from SCX, basic RP, and solution-IEF were identified, respectively. Basic RP and solution-IEF did provide good separation efficiency for the first dimensional peptide fractionation, and was suitable for coupling with a second dimensional acidic RP ESI MS/MS analysis. Orthogonal evaluation was accomplished by plotting each fractionation against the retention time for the nanoLC-MS/MS (low pH RP) analysis (SI Figure 4). Both fractionation strategies, SCX and solution-IEF, showed acceptable orthogonality. Basic RP fractionation, coupled with acidic conditions for conventional LC-MS/MS, provides only a limited orthogonality compared to the other two approaches. It is noteworthy that the early basic RP fractions showed an inconsistency for the orthogonal trend, which may be due to electrostatic interactions between peptides and water molecules under the conditions used. The final comparison was based on the total proteins identified in each of these three fraction strategies. Scaffold software was used to construct the diagrams (Figure 4) for the overlapping of proteins and peptides between approaches. A total of 3564 peptides were identified which were associated with 1127 proteins. The SCX, basic RP, and solution-IEF methods permitted a total of 60%, 64%, and 78% of proteins to be identified, respectively. The results for these approaches were complementary and allowed more than 20% more of proteins to be identified, when compared with a single fractionation strategy. Combining solution-IEF with basic RP fractionation permitted 93% of the total proteins to be identified in this study.

Differential Proteomic Results for CSC-like Cells

Differential protein expression was considered to be significant when the expression consistently increased or decreased with a fold change of 2 or more and a p value smaller than 0.05 by ProteinPilot analysis. Among the quantified proteins, the expression levels of 20 proteins were increased and 30 proteins were decreased compared with the controls. Detailed information such as accession number, gene symbol, averaged ratio, p values, and full protein names for these proteins are listed in Table 3.

We further analyzed these 50 differentially expressed proteins using the GeneGo database from CGAP (Cancer Genome Anatomy Project). All 50 gene symbols were functional annotation and enrichment by diseases (by Biomarkers) associated with liver diseases, hepatocellular carcinoma, and liver neoplasm. These values are not surprising, since the samples were obtained from a hepatocellular carcinoma cell line Hep3B. These gene symbols were also sent for GeneGo pathway maps analysis. The top ten pathways associated are metabolic pathways, cytoskeleton remodeling, and immune responses. Metabolic pathways are important for cellular functions and cell survival, and this indicates that unique metabolic pathways may be operative in CSC-like cells. Oxidative phosphorylation is related to cell apoptosis, and cell apoptosis may reflect the resistance of control cancer cells and CSC-like cells to drugs. Cytoskeleton remodeling and the regulation of the actin cytoskeleton by Rho GTPases are related to cell structure. Since the Hep3B clone 1 formed spheroids and clone 2 did not, the differential expression of cytoskeleton remodeling proteins can serve as a reflection of the structural difference between these two clones and further confirms the sensitivity of our analysis.

Table 5. Tumor Initiating Activities of the Two Clones of Hep3B Cells in SCID Mice[a]

	CD133	sphere form.	injected cell no.	no. of mice w/tumor on day 60
Hep3B	parental	partial	5×10^6	5/5
	CSC-like Hep3B	yes	3×10^3	5/5
	control Hep3B	no	3×10^3	0/5
	CSC-like Hep3B	yes	1×10^4	5/5
	control Hep3B	no	1×10^4	0/5
	CSC-like Hep3B	yes	1×10^5	5/5
	control Hep3B	no	5×10^6	0/5

[a]Different amounts of the two clones of Hep3B cells were injected into nude mice subcutaneously. The tumors formed on the injection sites were observed, and their dimensions were measured on day 60. The sizes of tumors were compared in control and CSC-like Hep3B cells, and the p-values were calculated by comparing the size of the tumors formed by control and CSC-like Hep3B cells.

To verify the data from iTRAQ, we sought to choose several genes. The S100 protein family comprises at least 21 different types of low molecular weight proteins. Members of this family are characterized by two calcium binding sites of the helix–loop–helix conformation. Functional aspects of the S100 proteins have been widely reported in several calcium dependent and independent intracellular activities. Extracellular roles of S100 proteins for various types of cells have also been reported.[21] In addition, S100P regulates cellular function through calcium dependent signaling pathways.[22] S100P was also reported to regulate cell adhesion and cell migration.[23] Although the expression of S100P is induced in intraductal papillary mucinous neoplasms and colorectal cancer, it was also reported that the expression of S100P is reduced at advanced stages of tumors.[24−26]

S100A14 was reported to regulate the invasive potential of squamous cell carcinoma and inhibit proliferation of oral carcinoma.[27,28] However, extracellular S100A14 shows dual roles in regulating the cell survival of esophageal squamous cell carcinoma (ESCC) cell lines. It stimulates cell proliferation at low doses and induces cell apoptosis at high doses.[29]

Vimentin is a type III intermediate filament that functionally supports and anchors organelles in cells. Therefore, it is an important component of the cytoskeleton. Since vimentin is expressed mostly in mesenchymal cells, it can serve as an

dx.doi.org/10.1021/pr4004294 | J. Proteome Res. 2013, 12, 3573−3585

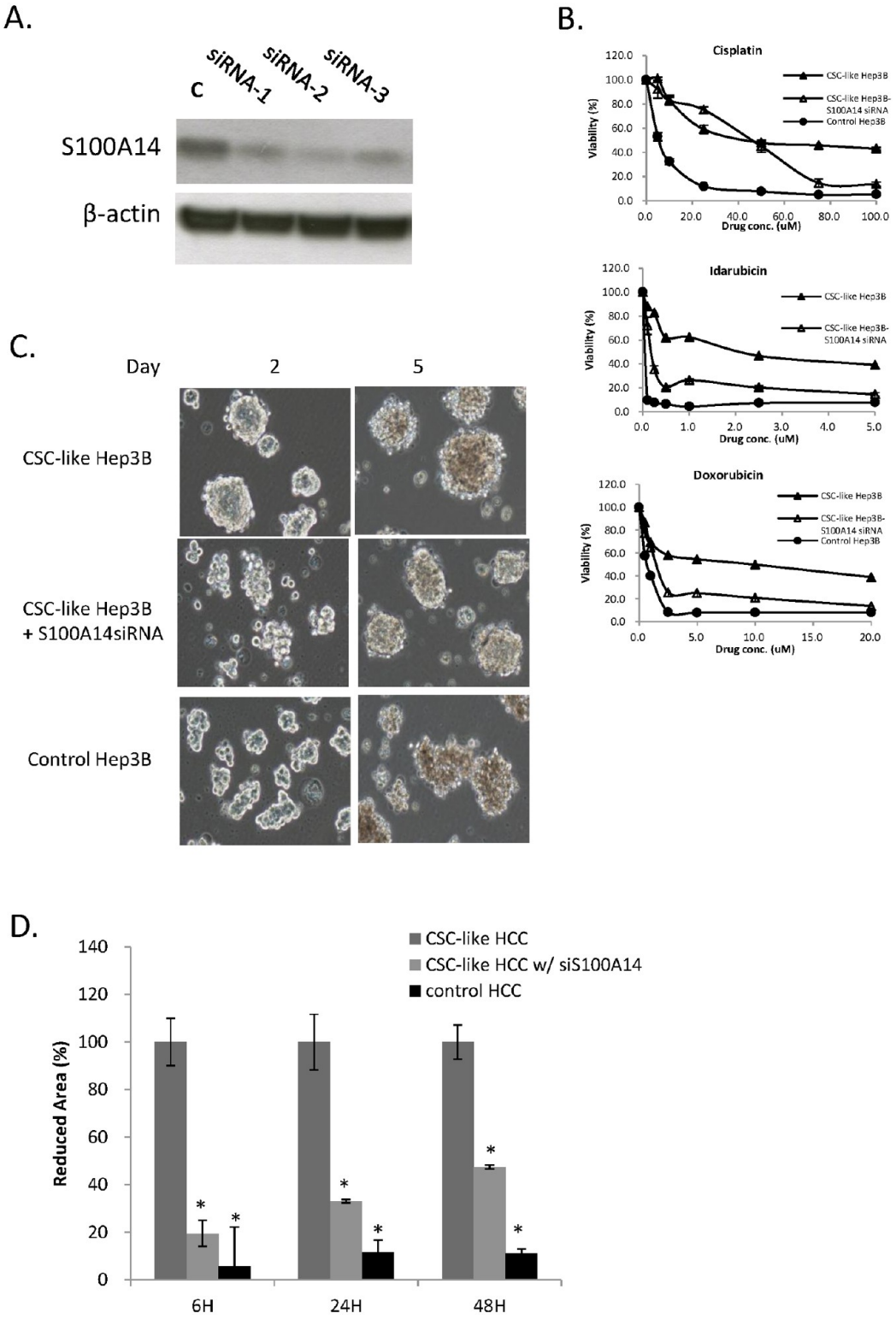

Figure 6. Functional importance of S100A14 in CSC-like Hep3B cells. (A) CSC-like Hep3B cells were treated with three different siRNA against S100A14. The expression levels of S100A14 in control and siRNA treated cells were shown. (B) Control Hep3B cells, CSC-like Hep3B cells, and siS100A14 treated CSC-like Hep3B cells were treated chemotherapeutic reagents. Cell viability of these Hep3B cells in each group was examined by MTT assay. (C) The abilities of spheroid formation in control, CSC-like, and siS100A14 treated CSC-like Hep3B cells were observed daily after cells were plated. Images of spheroid formation on day 2 and day 5 were shown. (D) Quantified results of the scratch assay were shown to show the cell motility of control, CSC-like, and siS100A14 treated CSC-like Hep3B cells ($N = 3$, $^*p < 0.05$).

important marker for epithelial-mesenchymal transition (EMT). Recent studies suggest that cancer stem cells proceed through dedifferentiation processes from specialized cells. The dedifferentiation process is related to the EMT process.[30] Indeed, the expression of vimentin is inversely correlated with the expression of CD24 in breast cancer cells, and low CD24 expression is

dx.doi.org/10.1021/pr4004294 | J. Proteome Res. 2013, 12, 3573−3585

considered to be an important marker for breast cancer stem cells.[31]

Therefore, S100P, S100A14, and vimentin were chosen to examine the expression level of these proteins in the two clones of Hep3B by QRT-PCR, FACS analysis, and/or Western blot. The relative expression patterns of all verified targets were consistent when detected by iTRAQ and QRT-PCR, FACS analysis, or Western blot (Figure 5A–C; SI Table 1).

Correlation of Identified Protein Expression and CSC-like HCC

The findings verify that S100P, S100A14, and vimentin are differentially expressed between control and CSC-like cells in Hep3B cell lines. We further examined the expression levels of these proteins in other hepatocellular carcinoma cell lines. The expression of these proteins in two other HCC cell lines, HepG2 and PLC/PRF/5, were monitored. The expression patterns of S100A14 and vimentin in PLC/PRF/5 were similar to those for CSC-like Hep3B cells, and the express patterns of these proteins in HepG2 were similar to those for control Hep3B (Figure 5D).

To study the stemness of these HCC cell lines, the resistance of these cells to chemotherapeutic drugs was examined. The resistance of PLC/PRF/5 was similar to that of CSC-like Hep3B cells, and they were more resistant to all the three chemotherapeutic reagents tested. On the contrary, HepG2 was similar to control Hep3B cells and was less resistant to these chemotherapeutic reagents (Table 4). In addition, the tumorigenicity of the two clones of Hep3B was tested in SCID mice (Table 5). As expected, CSC-like Hep3B cells formed tumors in SCID mice, but control Hep3B cells did not.

To functionally verify the importance of S100A14 in the CSC properties of Hep3B cells, we temporally repressed the expression of S100A14 in CSC-like Hep3B cells by siRNA treatments. The knockdown efficiency of siRNA treatment was verified (Figure 6A). Since siS100A14-2 showed the strongest knockdown efficiency, we treated CSC-like Hep3B cells with siS100A14-2 and functionally analyzed the stemness properties of these cells. First, the cell viability of control or siS100A14 treated CSC-like Hep3B cells in the presence of chemotherapeutic reagents was examined. Pretreatment of siS100A14 significantly sensitized CSC-like Hep3B cells toward chemotherapeutic reagents (Figure 6B). Second, spheroid formation was observed at as early as 2 days in CSC-like Hep3B cells. When CSC-like Hep3B cells were treated with siS100A14, cells did not form sphere until later (Figure 6C).

Finally, cell motility was examined in control Hep3B cells, CSC-like Hep3B cells, and CSC-like Hep3B cells treated with siS100A14. The results showed that knocking down S100A14 strongly inhibit Hep3B cell migration (Figure 6D). Based on these results, we propose that S100A14 is potentially a CSC marker for HCC cells and is functionally important for the CSC properties of HCC cells.

Consistent with published results, the expression level of vimentin was high in CSC-like Hep3B and low in control Hep3B cells. To functionally verify the importance of vimentin in the CSC properties of Hep3B cells, we treated the two clones of Hep3B with a vimentin inhibitor, withaferin A. Treatment of withaferin A repressed the expression of vimentin in CSC-like Hep3B cells (SI Figure 5A). To study the effect of vimentin on the drug resistance of CSC-like Hep3B cells, both clones of Hep3B were cotreated with withaferin A and chemotherapeutic reagents. The cotreatments of withaferin A and cisplatin synergistically suppressed the cell viability of CSC-like Hep3B but not control Hep3B cells. However, the synergistic effects were not observed when withaferin A treated cells were cotreated with doxorubicin or idarubicin (SI Table 2). In addition, pretreatment of withaferin A did not affect spheroid formation in CSC-like Hep3B cells (SI Figure 5B). However, since CSC-like Hep3B cells showed high cell motility (Figure 1D), we examined whether vimentin is important for cell migration in CSC-like Hep3B cells. CSC-like Hep3B cells were pretreated with withaferin A for 1 h before assay, and it was shown that the cell motility of CSC-like Hep3B cells was repressed in the withaferin A pretreated group (SI Figure 5C). Based on these results, inhibiting of vimentin partially affected the stemness properties of Hep3B cells. Therefore, we propose that vimentin could potentially be a cancer stem cell marker in certain types of cells.

■ CONCLUSIONS

CSC is a relatively new research topic in the field of cancer research. Considerable progress has been made in the CSC field in the past few years. As we gain more knowledge related to CSC, more questions arise that need to be solved. The ultimate goal of this study was to elucidate CSC associated pathways and molecules, which can potentially be used as biomarkers for CSC-like cells. However, due to the complexity of the nature of CSC, evaluating the "stemness" of cancer cells based on a single marker is a difficult task.

The expression patterns of multiple CSC markers can be used to predict CSC properties more precisely. Integrating analytical data from other CSC analysis platforms can strength the advantage. However, future studies will be conducted to evaluate the clinical significance of proteomic findings here for diagnostic and therapeutic applications of CSC in hepatocellular carcinoma.

■ ASSOCIATED CONTENT

Supporting Information

Figures and tables as described in the text. This material is available free of charge via the Internet at http://pubs.acs.org.

■ AUTHOR INFORMATION

Corresponding Author

*Phone: 886-2-77346210. Fax: 886-2-29324249. E-mail: sfchen@ntnu.edu.tw.

Author Contributions

‡C.-H.K. and C.-F.C. contributed equally to the present work.

Author Contributions

Conceived of and designed the experiments: C.-H.K., C.-F.C., L.-M.W., S.-F.C. Performed the experiments: C.-P.L., M.-W.L., S.-Y.W., C.-Y.S., H.-W.T., C.-C.W. Analyzed the data: T.-H.T., H.-W.T., Z.-K.K., C.-W.C. Wrote the paper: C.-H.K., C.-F.C., S.-F.C. All authors have given their approval to the final version of the manuscript.

Notes

The authors declare no competing financial interest.

■ ACKNOWLEDGMENTS

This work was supported by grants from the National Science Council of Taiwan, under Contracts NSC 98-2113-M-003-007-MY2 and NSC 100-2113-M-003-002-MY2.

■ ABBREVIATION:

CSC, cancer stem cells; HCC, hepatocellular carcinoma; iTRAQ, isobaric tags for relative and absolute quantitation

REFERENCES

(1) Jemal, A.; Siegel, R.; Xu, J.; Ward, E. Cancer statistics, 2010. *CA-Cancer J. Clin.* **2010**, *60* (5), 277−300.

(2) Reya, T.; Morrison, S. J.; Clarke, M. F.; Weissman, I. L. Stem cells, cancer, and cancer stem cells. *Nature* **2001**, *414* (6859), 105−11.

(3) Phillips, T. M.; McBride, W. H.; Pajonk, F. The response of CD24(-/low)/CD44+ breast cancer-initiating cells to radiation. *J. Natl. Cancer Inst.* **2006**, *98* (24), 1777−85.

(4) Chiba, T.; Kamiya, A.; Yokosuka, O.; Iwama, A. Cancer stem cells in hepatocellular carcinoma: Recent progress and perspective. *Cancer Lett.* **2009**, *286* (2), 145−53.

(5) Bantscheff, M.; Eberhard, D.; Abraham, Y.; Bastuck, S.; Boesche, M.; Hobson, S.; Mathieson, T.; Perrin, J.; Raida, M.; Rau, C.; Reader, V.; Sweetman, G.; Bauer, A.; Bouwmeester, T.; Hopf, C.; Kruse, U.; Neubauer, G.; Ramsden, N.; Rick, J.; Kuster, B.; Drewes, G. Quantitative chemical proteomics reveals mechanisms of action of clinical ABL kinase inhibitors. *Nat. Biotechnol.* **2007**, *25* (9), 1035−44.

(6) Ong, S. E.; Mann, M. Mass spectrometry-based proteomics turns quantitative. *Nat. Chem. Biol.* **2005**, *1* (5), 252−62.

(7) DeSouza, L.; Diehl, G.; Rodrigues, M. J.; Guo, J.; Romaschin, A. D.; Colgan, T. J.; Siu, K. W. Search for cancer markers from endometrial tissues using differentially labeled tags iTRAQ and cICAT with multidimensional liquid chromatography and tandem mass spectrometry. *J. Proteome Res.* **2005**, *4* (2), 377−86.

(8) Han, C. L.; Chien, C. W.; Chen, W. C.; Chen, Y. R.; Wu, C. P.; Li, H.; Chen, Y. J. A multiplexed quantitative strategy for membrane proteomics: opportunities for mining therapeutic targets for autosomal dominant polycystic kidney disease. *Mol. Cell. Proteomics* **2008**, *7* (10), 1983−97.

(9) Hsieh, H. C.; Chen, Y. T.; Li, J. M.; Chou, T. Y.; Chang, M. F.; Huang, S. C.; Tseng, T. L.; Liu, C. C.; Chen, S. F. Protein profilings in mouse liver regeneration after partial hepatectomy using iTRAQ technology. *J. Proteome Res.* **2009**, *8* (2), 1004−13.

(10) Lo, W. Y.; Wang, H. J.; Chiu, C. W.; Chen, S. F. miR-27b-regulated TCTP as a novel plasma biomarker for oral cancer: from quantitative proteomics to post-transcriptional study. *J. Proteomics* **2012**, *77*, 154−66.

(11) Jiang, F.; Qiu, Q.; Khanna, A.; Todd, N. W.; Deepak, J.; Xing, L.; Wang, H.; Liu, Z.; Su, Y.; Stass, S. A.; Katz, R. L. Aldehyde dehydrogenase 1 is a tumor stem cell-associated marker in lung cancer. *Mol. Cancer Res.* **2009**, *7* (3), 330−8.

(12) Tang, D. G.; Patrawala, L.; Calhoun, T.; Bhatia, B.; Choy, G.; Schneider-Broussard, R.; Jeter, C. Prostate cancer stem/progenitor cells: identification, characterization, and implications. *Mol. Carcinog.* **2007**, *46* (1), 1−14.

(13) O'Brien, C. A.; Pollett, A.; Gallinger, S.; Dick, J. E. A human colon cancer cell capable of initiating tumour growth in immunodeficient mice. *Nature* **2007**, *445* (7123), 106−10.

(14) Ma, S.; Chan, K. W.; Hu, L.; Lee, T. K.; Wo, J. Y.; Ng, I. O.; Zheng, B. J.; Guan, X. Y. Identification and characterization of tumorigenic liver cancer stem/progenitor cells. *Gastroenterology* **2007**, *132* (7), 2542−56.

(15) Zou, J.; Yu, X. F.; Bao, Z. J.; Dong, J. Proteome of human colon cancer stem cells: a comparative analysis. *World J. Gastroenterol.* **2011**, *17* (10), 1276−85.

(16) Dai, L.; Liu, Y.; He, J.; Flack, C. G.; Talsma, C. E.; Crowley, J. G.; Muraszko, K. M.; Fan, X.; Lubman, D. M. Differential profiling studies of N-linked glycoproteins in glioblastoma cancer stem cells upon treatment with γ-secretase inhibitor. *Proteomics* **2011**, *11* (20), 4021−8.

(17) Dai, L.; He, J.; Liu, Y.; Byun, J.; Vivekanandan, A.; Pennathur, S.; Fan, X.; Lubman, D. M. Dose-dependent proteomic analysis of glioblastoma cancer stem cells upon treatment with γ-secretase inhibitor. *Proteomics* **2011**, *11* (23), 4529−40.

(18) Lee, E. K.; Cho, H.; Kim, C. W. Proteomic analysis of cancer stem cells in human prostate cancer cells. *Biochem. Biophys. Res. Commun.* **2011**, *412* (2), 279−85.

(19) Dalerba, P.; Cho, R. W.; Clarke, M. F. Cancer stem cells: models and concepts. *Annu. Rev. Med.* **2007**, *58*, 267−84.

(20) Hermann, P. C.; Huber, S. L.; Herrler, T.; Aicher, A.; Ellwart, J. W.; Guba, M.; Bruns, C. J.; Heeschen, C. Distinct populations of cancer stem cells determine tumor growth and metastatic activity in human pancreatic cancer. *Cell Stem Cell* **2007**, *1* (3), 313−23.

(21) Donato, R. Intracellular and extracellular roles of S100 proteins. *Microsc. Res. Tech.* **2003**, *60* (6), 540−51.

(22) Yamaguchi, F.; Umeda, Y.; Shimamoto, S.; Tsuchiya, M.; Tokumitsu, H.; Tokuda, M.; Kobayashi, R. S100 proteins modulate protein phosphatase 5 function: a link between CA2+ signal transduction and protein dephosphorylation. *J. Biol. Chem.* **2012**, *287*, 13787.

(23) Du, M.; Wang, G.; Ismail, T. M.; Gross, S.; Fernig, D. G.; Barraclough, R.; Rudland, P. S. S100p dissociates myosin IIA filaments and focal adhesion sites to reduce cell adhesion and enhance cell migration. *J. Biol. Chem.* **2012**, *287*, 15330.

(24) Nakata, K.; Nagai, E.; Ohuchida, K.; Hayashi, A.; Miyasaka, Y.; Aishima, S.; Oda, Y.; Mizumoto, K.; Tanaka, M.; Tsuneyoshi, M. S100P is a novel marker to identify intraductal papillary mucinous neoplasms. *Hum. Pathol.* **2010**, *41* (6), 824−31.

(25) Ding, Q.; Chang, C. J.; Xie, X.; Xia, W.; Yang, J. Y.; Wang, S. C.; Wang, Y.; Xia, J.; Chen, L.; Cai, C.; Li, H.; Yen, C. J.; Kuo, H. P.; Lee, D. F.; Lang, J.; Huo, L.; Cheng, X.; Chen, Y. J.; Li, C. W.; Jeng, L. B.; Hsu, J. L.; Li, L. Y.; Tan, A.; Curley, S. A.; Ellis, L. M.; Dubois, R. N.; Hung, M. C. APOBEC3G promotes liver metastasis in an orthotopic mouse model of colorectal cancer and predicts human hepatic metastasis. *J. Clin. Invest.* **2011**, *121* (11), 4526−36.

(26) Rehbein, G.; Simm, A.; Hofmann, H. S.; Silber, R. E.; Bartling, B. Molecular regulation of S100P in human lung adenocarcinomas. *Int. J. Mol. Med.* **2008**, *22* (1), 69−77.

(27) Sapkota, D.; Bruland, O.; Costea, D. E.; Haugen, H.; Vasstrand, E. N.; Ibrahim, S. O. S100A14 regulates the invasive potential of oral squamous cell carcinoma derived cell-lines in vitro by modulating expression of matrix metalloproteinases, MMP1 and MMP9. *Eur. J. Cancer* **2011**, *47* (4), 600−10.

(28) Sapkota, D.; Costea, D. E.; Blø, M.; Bruland, O.; Lorens, J. B.; Vasstrand, E. N.; Ibrahim, S. O. S100A14 inhibits proliferation of oral carcinoma derived cells through G1-arrest. *Oral Oncol.* **2012**, *48* (3), 219−25.

(29) Jin, Q.; Chen, H.; Luo, A.; Ding, F.; Liu, Z. S100A14 stimulates cell proliferation and induces cell apoptosis at different concentrations via receptor for advanced glycation end products (RAGE). *PLoS One* **2011**, *6* (4), e19375.

(30) Mani, S. A.; Guo, W.; Liao, M. J.; Eaton, E. N.; Ayyanan, A.; Zhou, A. Y.; Brooks, M.; Reinhard, F.; Zhang, C. C.; Shipitsin, M.; Campbell, L. L.; Polyak, K.; Brisken, C.; Yang, J.; Weinberg, R. A. The epithelial-mesenchymal transition generates cells with properties of stem cells. *Cell* **2008**, *133* (4), 704−15.

(31) Morel, A. P.; Lièvre, M.; Thomas, C.; Hinkal, G.; Ansieau, S.; Puisieux, A. Generation of breast cancer stem cells through epithelial-mesenchymal transition. *PLoS One* **2008**, *3* (8), e2888.